Pergamon

Geochimica et Cosmochimica Acta, Vol. 60, No. 12, pp. 2219–2232, 1996

0016-7037/96 $15.00 + .00

PII S0016-7037(96)00080-4

A geochronological $^{40}Ar/^{39}Ar$ and $^{87}Rb/^{87}Sr$ study of K-Mn oxides from the weathering sequence of Azul, Brazil

G. RUFFET,[1] C. INNOCENT,[2] A. MICHARD,[2] G. FÉRAUD,[1] A. BEAUVAIS,[3] D. NAHON,[2] and B. HAMELIN[2]

[1]Institut de Géodynamique, URA CNRS 1279, Université de Nice-Sophia Antipolis, 06108 Nice Cedex 2, France
[2]Laboratoire de Géosciences de l'Environnement, URA CNRS 132, CEREGE, Europôle Méditerranéen de l'Arbois, BP80, 13545 Aix-en-Provence Cedex 4, France
[3]ORSTOM (UM GECO) Department of Geology, University of Washington, Seattle, WA 98195, USA

(*Received July* 12, 1995; *accepted in revised form February* 26, 1996)

Abstract—K-Mn oxides of hollandite group minerals such as cryptomelane ($K_{1-2}(Mn^{3+}, Mn^{4+})_8O_{16}nH_2O$) are often precipitated authigenically in weathering profiles. The presence of structural K allows these minerals to be dated by the K-Ar and $^{40}Ar/^{39}Ar$ methods, making it possible to study the progression of oxidation fronts during weathering processes. Within the context of a recent $^{40}Ar/^{39}Ar$ study of cryptomelane from the Azul Mn deposit in the Carajàs region (Amazônia, Brazil), Vasconcelos et al. (1994) defined three age clusters (65–69, 51–56, and 40–43 Ma) and proposed that they correspond to the episodic precipitation of the three generations of Mn oxide that have been identified in the deposit (Beauvais et al., 1987).

We performed a laser probe $^{40}Ar/^{39}Ar$ and $^{87}Rb/^{87}Sr$ study on new samples from the same Mn deposit. Our $^{40}Ar/^{39}Ar$ data confirm that cryptomelane is a suitable mineral for $^{40}Ar/^{39}Ar$ dating, although in some cases we clearly identify the existence of ^{39}Ar recoil effects. Although the corresponding age spectra are generally strongly disturbed, our results also confirm that the earliest cryptomelane generation is of Upper Cretaceous-Paleocene age. We obtained good plateau ages from veins and concretions of the second cryptomelane generation. Some of these results allow definition of a well-constrained age cluster at 46.7–48.1 Ma not observed by Vasconcelos et al. (1994). A petrographic study confirms that none of the samples analyzed in the present study contained material associated with the third generation of cryptomelane. We propose that these new results support the idea of a more or less continuous crystallization of K-Mn oxides, mainly constrained by local factors, rather than the model advanced by Vasconcelos et al. (1994), which suggests that each cryptomelane generation corresponds to distinct weathering events related to global climatic changes.

$^{87}Sr/^{86}Sr$ data show large variations, clearly inherited from the 2.1 Ga parent rock of the Mn protore. The Rb/Sr results demonstrate that minimum fractionation occurs during cryptomelane crystallization, except for the latest generation, which is depleted in Sr. This precludes use of the Rb/Sr radiochronometer for dating secondary Mn oxides in laterites.

1. INTRODUCTION

Weathering is one of the main processes in the geomorphologic and geochemical evolution of the Earth's surface. Lateritic terrains, which represent approximately one third of the continental surface and form the substrate of equatorial forests, are the end-products of long-term exposure of cratonic rocks under tropical climate. The precise determination of the rate of continental crust weathering is thus a critical parameter for soil sciences and paleoclimatology. However, direct dating of weathering phenomena remained a very difficult problem until recently. The open-system evolution of most weathering profiles precludes direct radiochronological dating using most standard radiometric techniques. Hence, current studies focus on the search for supergene minerals, which may behave as closed systems for at least one isotopic chronometer.

K-bearing supergene minerals such as alunite and jarosite, or K-Mn oxides of the hollandite group such as cryptomelane, are widely present in soils and weathering profiles. Cryptomelanes are important components of Mn-bearing laterites from West Africa (Nahon et al., 1984; Perseil and Grandin, 1985) and Brazil (Herz and Banerjee, 1973; Beauvais et al., 1987). Vasconcelos et al. (1994) showed that cryptomelane and hollandite are potentially suitable minerals for dating weathering processes by the K-Ar and $^{40}Ar/^{39}Ar$ methods. Their $^{40}Ar/^{39}Ar$ results yielded internally consistent results for a series of distinct cryptomelane generations formed during lateritization of Archean and Proterozoic bedrocks in the Carajás Region, Amazonia (Brazil), and led to the proposition that the three age clusters were associated with distinct crystallization events correlated with major environmental changes and climatic periods. These results gave thus the first absolute time constraints on the rate of development of laterite sequences.

The aims of the present work are (1) to discuss the analytical problems which can be encountered during $^{40}Ar/^{39}Ar$ laser-probe analyses of cryptomelanes, (2) to add new $^{40}Ar/^{39}Ar$ results to one of the profiles studied by Vasconcelos et al. (1994), in order to improve the statistical significance of the age distribution of the Mn oxides at this site, (3) to test whether the various cryptomelane generations are related to major environmental changes, or to continuous weathering with various stages related to differences in weathering rates of the minerals forming the source rock, and (4) to determine whether cryptomelanes also behave as a closed system for Rb-Sr. Coupled K-Ar and $^{87}Rb/^{87}Sr$ studies have been successfully applied previously to some phyllosilicates like

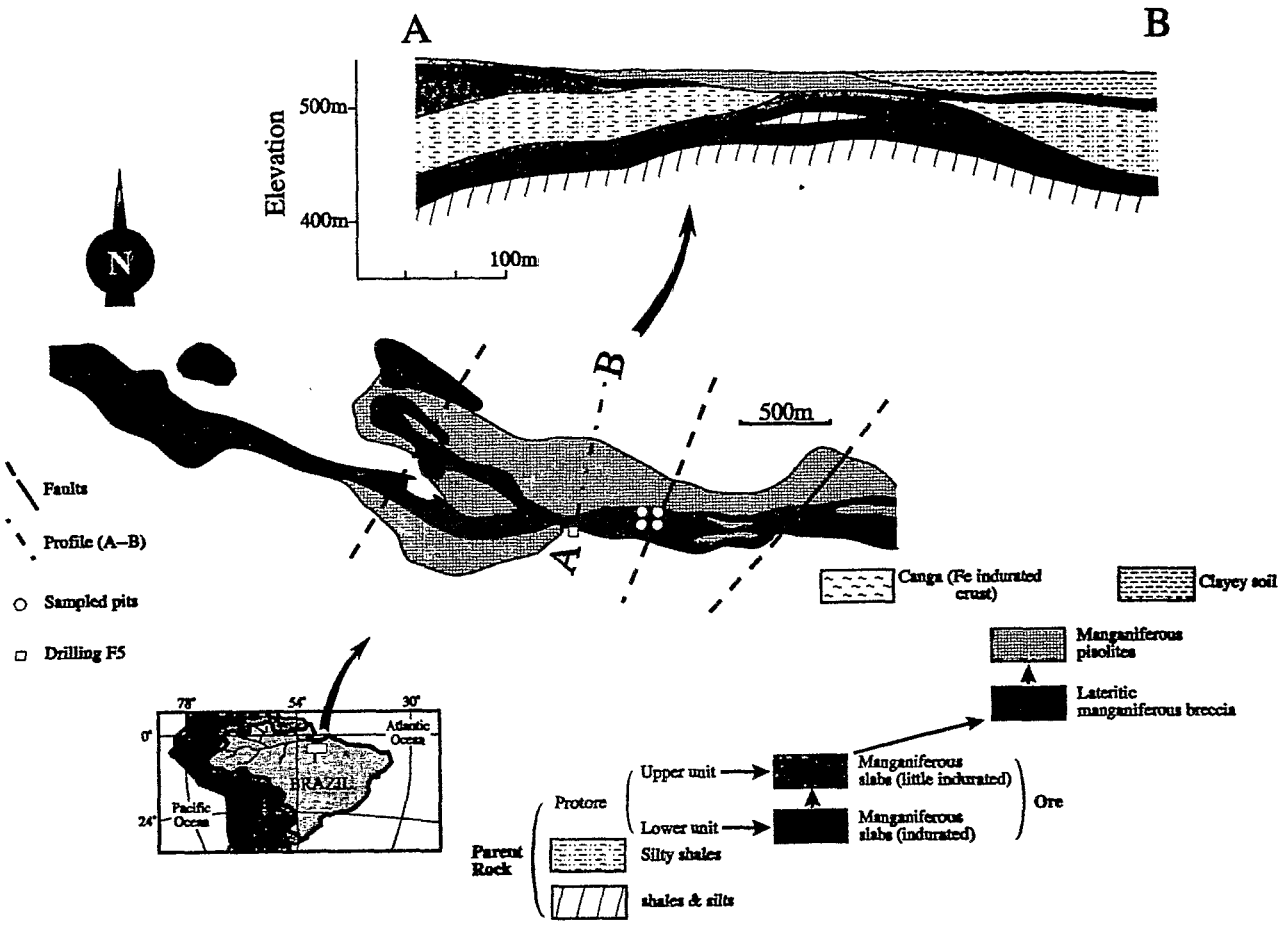

FIG. 1. Geological map and profile (labelled A–B on map) of the Azul ore deposit (after Bernardelli and Beisiegel, 1978) with the location of the four shafts (described by Beauvais (1984)) in which samples were handpicked for this study. Drilling F5 reaches the fresh (unweathered) parent rock.

glauconites (Morton and Long, 1980), smectites (Clauer et al., 1984), celadonites (Staudigel et al., 1986), and illites (Clauer et al., 1993). The crystallographic structure of cryptomelane may host Rb as well as K, and thus cause large fractionation of the Rb/Sr ratio. Fifteen new samples from the Azul Mn-ore (Carajàs mountains, Para state, Brazil), one of the sites previously studied by Vasconcelos et al. (1994), were analyzed with the Rb/Sr and $^{40}Ar/^{39}Ar$ methods.

2. SAMPLES

2.1. Geological Setting and Sampling

The Azul Mn-ore is located near the Fe deposit of Carajàs (Para State, Brazil) at about 500 km south of Belem. It developed on Lower Precambrian sedimentary shales (Rio Fresco Group). The weathering sequence consists of four main horizons (Fig. 1): the relics of the non-manganiferous parent rock horizon (shales and silts); the Mn-oxides "plaquettes" horizon (manganiferous indurated and little indurated slabs); the brecciated Mn-oxides horizon (lateritic manganiferous breccia), and the pisolitic horizon (manganiferous pisolites).

The parent rock was reached by drilling to a depth of 100 m (Drilling F5, Fig. 1). The oxidized horizons were sampled in several pits, about 40 m deep, which reached various horizons along the slope of the plateau.

Samples were collected from the four profiles (Fig. 1) described by Beauvais (1984), approximately 300 m away from the section studied by Vasconcelos et al. (1994). Locations and description of the samples are reported in the Appendix. Fifteen samples were analyzed, corresponding to eight whole-ore samples collected in the different units, five "separates" extracted from veins or concretions (labeled by "II" after the reference of the corresponding whole-ore), one sample of lithiophorite (#22-III), and one clay matrix (#15-III). The whole-ore samples range from dark bluish metallic blocks to dull-black, more friable pieces. Two of the "separates" come from millimetric veins visible in polished whole-ore sections (#22-II and #32-II), one (#28-II) from a light-grey metallic rim, one millimeter thick, on the faces of a fissure, and two (#7-II and #31-II) from brownish submillimetric botryoïdal rim covering the faces of fissures. All of the analyzed samples are essentially composed of cryptomelane, although X-ray diffraction reveals the presence of small amounts of nsutite and pyrolusite.

2.2. Mineralogical Evidence for Successive Generations of Mn Oxides

The Azul profile is composed of different generations of Mn oxides, among which, several generations of cryptomelane have been differentiated (Beauvais et al., 1987).

The parent rock is composed of 65% rhodochrosite, 15% phyllosilicates, 10% quartz, 5% feldspars, and 5% sulfides. The rhodochrosite consists of "egg-fish" shaped micronodules of tiny crystals (2–10 μm) or of sparitic crystals (50 μm), located in veins crossing the bedding of the shale. The chemical composition of the rhodochrosite,

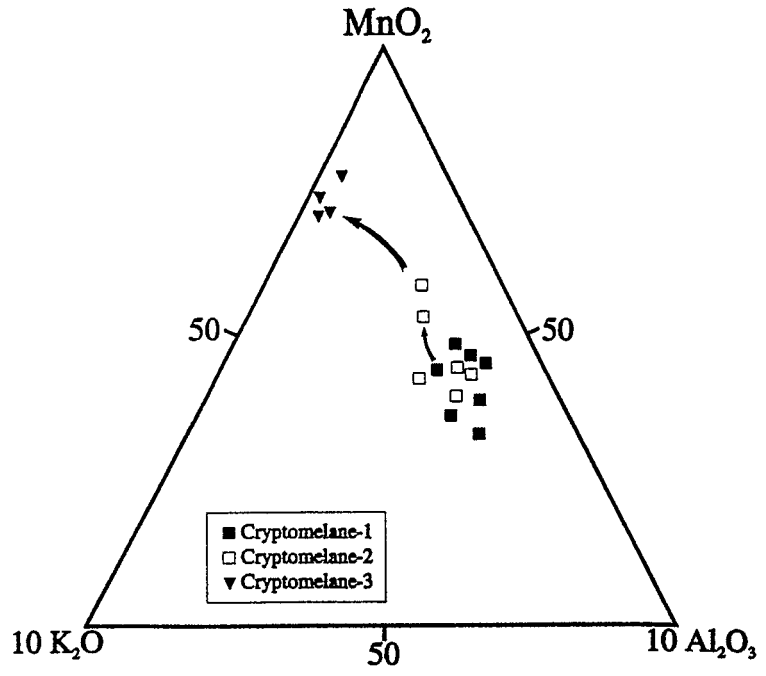

FIG. 2. Chemical compositions of different generations of cryptomelane plotted in a $MnO_2-10K_2O-10Al_2O_3$ triangular diagram.

obtained from microprobe analyses by Beauvais et al. (1987) (fifteen analyses) is:

$$(Mn^{2+}_{0.93}Fe^{2+}_{0.04}Mg_{0.01}Ca_{0.02})CO_3.$$

The X-ray diffraction pattern is: 3.660 Å; 2.840 Å; 2.386 Å; 2.169 Å; 1.998 Å; 1.825 Å; 1.760 Å; and 1.538 Å. Quartz grains are mostly detrital grains (20–50 μm), but can also occur as euhedral crystals (100–200 μm), in association with veins of rhodochrosite. Phyllosilicates are detrital grains of muscovite and chlorite, ranging in size from 10 to 30 μm. Feldspars (<50 μm) are K-feldspars. Sulfides consist of pyrite and covellite, as euhedral crystals, along with rhodochrosite.

The Mn-oxides "plaquette" horizon results from weathering of the two different units of rhodochrosite-bearing shales of the Rio Fresco Group. The original rhodochrosite weathers directly into a first generation of cryptomelane (thereafter labeled "cryptomelane-1"). The chemical composition of cryptomelane-1 is shown on a triangular diagram (Fig. 2) (Beauvais et al., 1987) (seven analyses; sample #1). The main X-ray patterns are 6.90 Å, 4.90 Å, 2.39 Å, and 2.14 Å. The cryptomelane structure consists of a framework of double chains of edge-sharing Mn-O octahedra containing large tunnels filled with K^+ ions. Most of the Mn is Mn^{4+} but some Mn^{3+} substitutes for Mn^{4+} to balance the positive charge of tunnel cations (Post et al., 1982; Hypólito et al., 1984). The composition is $K_xMn^{4+}_{8-x}Mn^{3+}_xO_{16}$ (Vicat et al., 1986), with x ranging from 0.2 to 1.0 in cryptomelanes from lateritic profiles.

Cryptomelane-1 consists of tiny aggregated crystals (up to a few tens micrometers) that pseudomorphically replace rhodochrosite grains. This is manifested by the preservation of the original sedimentary structure of the parent rock, and of the original fish-egg shape of the nodules (Fig. 3). The strong increase in density implies that pseudomorphic replacement of rhodochrosite by cryptomelane-1 requires a net import of Mn (Beauvais et al., 1987; Merino et al., 1993).

Direct pseudomorphs of rhodochrosite by cryptomelane have been already observed at Moanda (Gabon) (Nziengui-Mapangou, 1981), although direct replacement of rhodochrosite by manganite (MnOOH) is more commonly observed. Recent thermodynamic studies (Parc et al., 1989; Nahon and Parc, 1990) have shown that manganite is not stable for high CO_2 pressures ($\log f CO_2 > -2.0$) and that cryptomelane can form directly from weathering of Mn carbonates at sufficient K^+ concentrations ($\log [K^+]/[H^+] > 3$).

Cryptomelane-1 and nsutite (a more highly oxidized mineral containing less Mn3+), can be intermingled in samples and are generally difficult to separate (Fig. 3). The nsutite formula is $Mn^{4+}_{1-y}Mn^{3+}_yO_{2-y}(OH)_y$ with $y < 0.05$ (Giovanoli and Leuenberger, 1969).

FIG. 3. Reflected light (×4): C1 is the first generation of cryptomelane (cryptomelane-1) associated with few nsutite in pseudomorph after the parent rock. Notice that they preserved the original microlaminated and egg-fish texture. C2 is the second generation of cryptomelane (cryptomelane-2) along with few nsutite, crossing the C1. Sample #28.

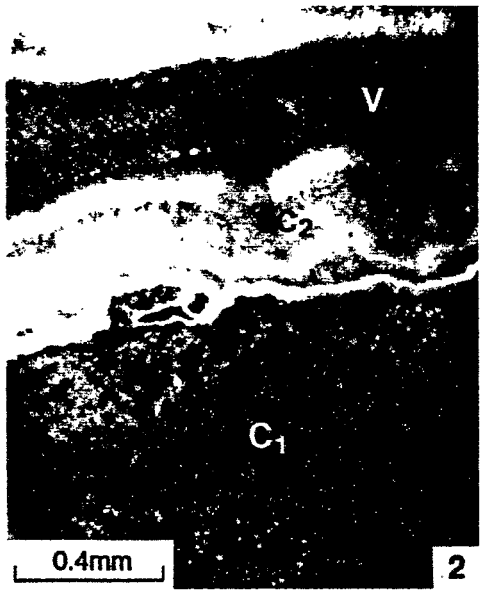

FIG. 4. Reflected light (×4): Fibroradiated crystals of cryptomelane-2. V is void and C1 is cryptomelane-1 with preserved original texture. Sample #31.

The walls of open fissures or microscopic tubules, crossing the fish-egg texture, often show recrystallization of nsutite and cryptomelane into a new generation of cryptomelane-2 and nsutite-2 (Figs. 3, 4). Recrystallization is indicated by the fact that (1) the fish-egg microtexture is now erased and (2) that cryptomelane-2 and nsutite-2 show fibroradiated crystals perpendicular to the walls of the fissures and tubules (Fig. 4). This second generation of cryptomelane-2 is slightly enriched in K. It is generally very difficult to separate completely cryptomelane-1 from cryptomelane-2, in which tiny remnants of cryptomelane-1 can persist.

Higher in the weathering profile, i.e., in more oxidized environments, pyrolusite (well-ordered MnO_2) replaces cryptomelane-2 and nsutite-2 in the same structural position. Pyrolusite is thus the final end-product of the weathering sequence (Bricker, 1965; Garrels and Christ, 1965). However, at the stage where pyrolusite precipitates, most detrital muscovite grains (15% of the parent rock) are not yet entirely weathered into kaolinite (Fig. 5). K-micas persist in the upper part of the weathering profile because K^+ cations are more solidly bound to the muscovite structure than they are in K-feldspars, which weather as soon as the weathering front develops. Thus, K^+ ions released during the early dissolution of detrital K-feldspars lead to the formation of cryptomelane-1 and cryptomelane-2, while leaching of interlayer K from detrital muscovite grains occurs after the precipitation of pyrolusite, and leads to the late destabilization of MnO_2 into a new generation of cryptomelane-3 (Beauvais et al., 1987; Vasconcelos et al., 1994). Well-developed crystals of pyrolusite (~100 μm), observed in the upper part of the weathering profile of Azul, show dissolution features on their faces. Cryptomelane-3 precipitates as tiny needles in these dissolution voids and progressively replaces the whole pyrolusite (Fig. 6). The shape of the original pyrolusite can be preserved through this pseudomorphic replacement by cryptomelane-3.

It is important to stress that, in contrast with the samples studied by Vasconcelos et al. (1994), none of the samples analyzed in the present study contained cryptomelane-3.

Finally, when muscovite is entirely weathered into kaolinite, Al released by kaolinite weathering can feed lithiophorite formation at the top of the profile.

3. ANALYTICAL TECHNIQUES

Massive samples were sawed. The veins were extracted from the whole ore either with a small handsaw or with metal tweezers. The lithiophorite was scraped out with a clean needle. The kaolinitic clay was separated away from the ore by vibrating the sample in an ultrasonic bath and pouring off the suspendant. All samples were rinsed several times in distilled water in an ultrasonic bath.

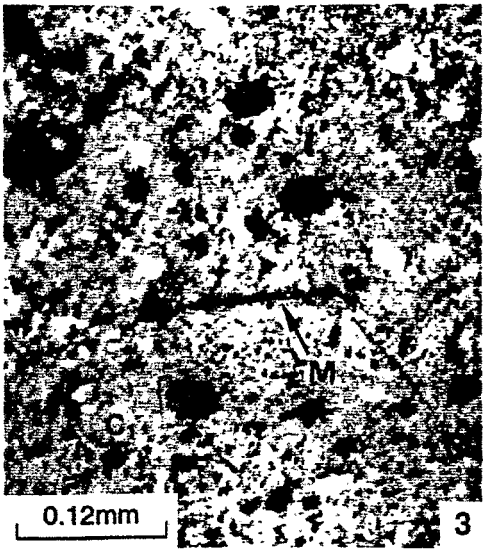

FIG. 5. Reflected light (×16): M is a detrital muscovite grain within the cryptomelane-1 (C1). Sample #32.

3.1. Rb-Sr Method

Samples of about 10 mg were dissolved in concentrated HCl (5 mL) and spiked with ^{84}Sr and ^{85}Rb. The clay was dissolved in a $HF-HNO_3-HClO_4$ mixture (5 mL). All samples were then dried and redissolved in aqua regia (1 mL), dried again, and finally dissolved in a few drops of dilute HCl. Rubidium was collected by precipitating Rb perchlorates and Sr was eluted on a AG50W X8 cation column (Alibert et al., 1983).

Rubidium and Sr were loaded on single W filaments with Ta oxide and run on a VG Sector 54-30 mass spectrometer. Strontium

FIG. 6. SEM observation P is a crystal of pyrolusite. Along the cracks and fissures crossing pyrolusite, needles of cryptomelane develop. This is the third generation of cryptomelane (C3). V is void. In Beauvais et al. (1987)

Table 1. Rb/Sr data

Sample	Lithology	Rb (ppm)	Sr (ppm)	1/Sr (ppm)	$^{87}Rb/^{86}Sr$	$^{87}Sr/^{86}Sr$	2σ
#1	Whole-ore	24.34	142.05	0.0070	0.684	0.766860	0.000010
#7	Whole-ore	23.83	138.99	0.0072	0.684	0.752736	0.000009
#7-II	Concretion	25.80	159.33	0.0063	0.646	0.751376	0.000008
#15	Whole-ore	24.16	109.46	0.0091	0.880	0.762337	0.000007
#22	Whole-ore	62.83	105.53	0.0095	2.375	0.813724	0.000010
#22-II	Vein	68.79	153.96	0.0065	1.782	0.811822	0.000043
#22-III	Lithiophorite	41.39	179.99	0.0056	0.917	0.795445	0.000013
#28	Whole-ore	49.41	160.45	0.0062	1.228	0.789596	0.000006
#28-II	Vein	60.70	43.59	0.0229	5.554	0.811186	0.000009
#31	Whole-ore	37.99	296.36	0.0034	0.511	0.759074	0.000008
#31-II	Concretion	61.86	75.41	0.0133	3.272	0.795461	0.000012
#32	Whole-ore	18.81	442.19	0.0023	0.170	0.744916	0.000008
#32-II	Vein	26.81	502.91	0.0020	0.213	0.745237	0.000012
#34	Whole-ore	27.72	546.52	0.0018	0.202	0.747518	0.000014
#34 Dupl.	Whole-ore	24.87	659.36	0.0015	0.150	0.746628	0.000008

Rubidium and Sr concentrations and strontium isotopic compositions of the analysed samples.

isotopes were measured using a dynamic multicollection mode. Repeated analyses of NBS 987 standard gave an average value of: 0.710205 ± 16 ($2\sigma_m$ on twenty-four runs). Strontium total blanks were negligible, lower than 300 pg.

3.2. $^{40}Ar/^{39}Ar$ method

The grains analyzed with the laser probe were carefully hand-picked under a binocular microscope from coarse fractions (0.5–2 mm) of the crushed samples. The samples were irradiated at the McMaster reactor (Hamilton, Canada) with a total flux of 9×10^{18} $n.cm^{-2}$. All of the analyzed samples were gathered in a narrow zone at the same level within the irradiation can in order to minimize the effect of the flux gradient, which is estimated to be less than ±0.5%. The irradiation standard was the amphibole MMhb1 (Samson and Alexander, 1987; 520.4 Ma).

The step-heating experiments on single grains (described in detail by Scaillet et al., 1990; Ruffet et al., 1991) were performed with a laser-probe using a Coherent Innova 70-4 continuous Ar-ion laser model with a maximum output power of 6 Watts in multiline mode. The laser beam was focused through an optical system onto a sample located in a UHV sample chamber (a Cu sample-holder, beneath a Pyrex window, in a stainless steel chamber).

Each laser experiment lasts 5 min: (1) 3 min in the purification line (laser heating of the sample and cleanup of the released gas) and (2) 2 min of inlet time into the mass spectrometer. The laser beam size is at least 2.5 times greater (up to 6 mm) than the sample size, in order to obtain a homogeneous temperature over the whole grain. The temperature is not known but its homogeneity is controlled by observing the heated mineral with a binocular microscope, coupled with a color video camera and a high resolution video recorder. The laser heating time (1 min) is kept constant for each step-heating experiment. The fusion of the mineral is achieved by sharply focusing the laser spot.

The mass spectrometer consists of a 120° M.A.S.S.E.® tube, a Bäur Signer® source, and an SEV 217® electron-multiplier (total gain: 5×10^{12}). The purification line comprises an SAES GP50W getter with St101® Zr Al alloy operating at 400°C and

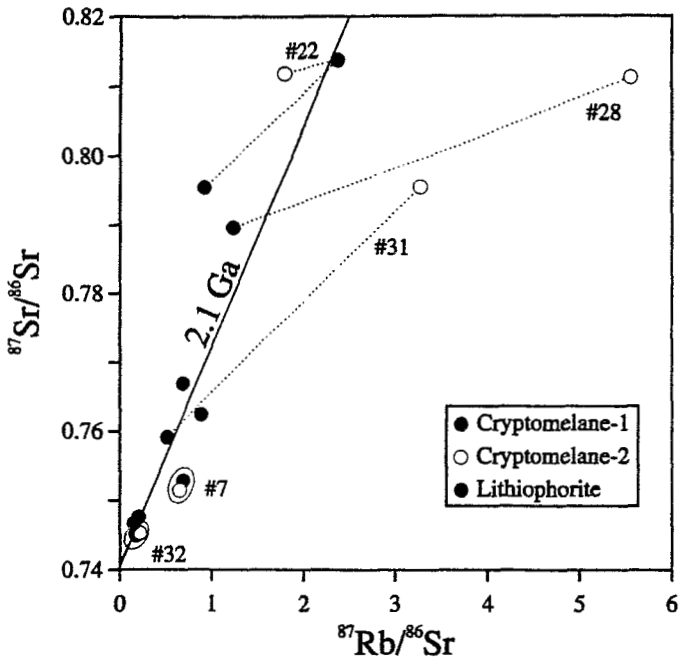

FIG. 7. Diagram $^{87}Sr/^{86}Sr$ vs. $^{87}Rb/^{86}Sr$ with 2.1 Ga reference isochrone.

TABLE 2. $^{40}Ar/^{39}Ar$ analytical data

Step n°	$^{40}Ar_{atm.}$ (%)	$^{39}Ar_K$ (%)	$^{37}Ar_{Ca}/^{39}Ar_K$ ($\times 10^{-4}$)	$^{40}Ar^*/^{39}Ar_K$	Age (Ma)
#1 Cryptomelane (Single grain) (J=0.0164325)					
1	91.1	0.36	0.0280	1.65	48.3 ± 40.7
2	79.4	3.77	0.0688	1.71	49.9 ± 4.9
3	59.0	3.64	0.0918	1.55	45.3 ± 5.3
4	67.1	3.04	0.0845	1.01	29.8 ± 6.6
5	60.0	5.62	0.0961	1.14	33.3 ± 3.6
6	24.5	23.01	0.0515	2.09	60.8 ± 1.3
7	9.4	14.82	0.0311	2.29	66.7 ± 1.4
8	8.5	19.76	0.0388	2.17	63.1 ± 1.1
9	20.5	19.43	0.0923	1.29	37.9 ± 1.1
10	27.7	5.08	0.0987	1.20	35.1 ± 2.8
Fuse	41.0	1.48	0.1072	1.00	29.4 ± 12.7
				Total age:	52.4 ± 0.7
#7 Cryptomelane (Single grain) (J=0.0164325)					
1	75.0	61.86	0.0743	1.72	50.3 ± 2.4
2	42.0	11.35	0.0494	1.48	43.3 ± 2.2
3	64.0	9.76	0.1178	0.68	20.2 ± 2.7
4	53.4	13.36	0.1339	0.54	15.9 ± 2.1
5	66.1	2.04	0.0522	1.01	29.6 ± 8.9
6	72.6	0.61	0.0000	0.60	17.6 ± 34.9
Fuse	76.2	1.02	0.0451	0.54	15.8 ± 21.2
				Total age:	41.0 ± 1.6
#7 Cryptomelane (Single grain) (J=0.0164325)					
1	34.5	3.78	0.2075	1.28	37.7 ± 1.7
2	49.5	5.20	0.0836	1.28	37.5 ± 1.9
3	36.7	4.75	0.1785	1.20	35.2 ± 1.9
4	9.8	8.84	0.1339	1.28	37.6 ± 1.1
5	5.8	24.22	0.0920	1.47	43.0 ± 0.5
6	5.2	14.75	0.0865	1.68	49.2 ± 0.5
7	5.8	7.94	0.0598	1.67	49.0 ± 0.9
8	6.0	11.30	0.0707	1.45	42.5 ± 0.6
9	6.9	14.43	0.1124	0.90	26.4 ± 0.7
Fuse	17.8	4.78	0.1197	0.90	26.5 ± 2.5
				Total age:	39.8 ± 0.3
#7-II Cryptomelane (Single grain) (J=0.0164325)					
1	96.7	0.78	0.1461	0.58	17.2 ± 19.7
2	80.2	6.08	0.0383	1.08	31.8 ± 4.0
3	71.4	7.37	0.0348	1.36	39.9 ± 3.2
4	44.2	13.38	0.0196	1.63	47.6 ± 1.4
5	18.9	20.24	0.0159	1.63	47.8 ± 0.8
6	15.3	17.77	0.0106	1.62	47.5 ± 0.9
7	20.8	10.98	0.0260	1.56	45.8 ± 1.1
8	38.4	8.60	0.0565	1.33	38.9 ± 1.6
Fuse	16.4	14.79	0.0145	1.42	41.5 ± 0.9
				Total age:	44.0 ± 0.5
#15 Cryptomelane (Single grain) (J=0.0164325)					
1	96.9	0.04	0.0000	0.50	14.8 ± 71.8
2	93.4	3.48	0.0626	2.00	58.2 ± 5.5
3	49.8	2.87	0.0472	2.61	75.7 ± 2.0
4	42.4	4.22	0.0377	2.67	77.6 ± 1.5
5	17.5	6.94	0.0342	2.61	75.9 ± 1.0
6	8.8	9.57	0.0240	2.31	67.2 ± 0.7
7	5.6	19.39	0.0199	2.21	64.4 ± 0.4
8	4.8	28.27	0.0182	2.15	62.7 ± 0.2
9	7.9	13.65	0.0217	2.10	61.3 ± 0.4
10	35.8	4.01	0.0544	2.22	64.6 ± 1.1
11	14.6	2.62	0.0438	2.80	81.2 ± 1.3
Fuse	28.9	4.94	0.0331	2.14	62.3 ± 1.1
				Total age:	65.5 ± 0.3
#22 Cryptomelane (Single grain) (J=0.0164325)					
1	99.0	0.41	0.1192	1.18	34.6 ± 55.4
2	97.9	3.41	0.1033	1.14	33.4 ± 9.4
3	96.9	5.60	0.0968	1.27	37.3 ± 8.2
4	95.3	6.76	0.0930	1.22	35.9 ± 5.0
5	86.6	8.99	0.0499	1.83	53.3 ± 2.0
6	58.1	15.36	0.0447	2.30	67.0 ± 1.8
7	43.8	19.28	0.0390	2.32	67.5 ± 1.0
8	39.0	16.61	0.0258	2.37	68.8 ± 0.9
9	35.7	7.66	0.0202	2.71	78.5 ± 1.3
10	33.1	5.55	0.0112	5.04	143.5 ± 2.0
11	40.4	3.91	0.0273	11.71	317.5 ± 4.1
Fuse	65.7	6.46	0.0389	4.00	114.9 ± 1.7
				Total age:	79.1 ± 0.8
#22-II Cryptomelane (Single grain) (J=0.0164325)					
1	34.0	13.46	0.1232	1.35	39.5 ± 1.4
2	13.7	10.83	0.1313	1.56	45.6 ± 0.9
3	4.7	9.83	0.1760	1.94	56.5 ± 1.1
4	3.4	41.92	0.0409	2.24	65.1 ± 0.3
5	1.4	14.05	0.0314	3.30	95.2 ± 0.8
6	1.5	3.11	0.0837	20.45	522.6 ± 4.5
Fuse	1.4	6.79	0.0000	6.96	195.4 ± 1.9
				Total age:	86.1 ± 0.4

$^{40}Ar_{atm}$ = atmospheric ^{40}Ar. $^{40}Ar^*$ = radiogenic ^{40}Ar. Ca = produced by Ca-neutron interferences. K = produced by K-neutron interferences. Age (Ma) = the date is calculated using the decay constants recommended by Steiger and Jager (1977). The error is at the 1σ level and does not include the error in the value of the J parameter. Correction factors for interfering isotopes produced by neutron irradiation were $(^{39}Ar/^{37}Ar)_{Ca} = 7.0 \times 10^{-4}$, $(^{40}Ar/^{39}Ar)_{Ca} = 2.8 \times 10^{-4}$, $(^{40}Ar/^{39}Ar)_K = 2.58 \times 10^{-2}$.

a −95°C cold trap. Static measurements of argon isotopes correspond to eleven peak hopping scans. Backgrounds of the extraction and purification laser system were measured every first or third step and subtracted from each argon isotope from the subsequent gas fraction(s). Typical blank values were $2.7 \times 10^{-12} < M/e40 < 1.0 \times 10^{-11}$ and $1.0 \times 10^{-13} < M/e36 < 3.8 \times 10^{-13}$ cm^{-3} STP.

All isotopic measurements are corrected for potassium and calcium isotopic interferences, mass discrimination, and atmospheric argon contamination. All errors are quoted at the 1σ level and do not include the errors on the $^{40}Ar^*/^{39}Ar_K$ ratio and age of the monitor. The error on the $^{40}Ar^*/^{39}Ar_K$ ratio of the monitor is included in the calculation of the plateau age error bars. To define a plateau age, we need at least three consecutive steps, corresponding to a minimum of 70% of the total $^{39}Ar_K$ released, and the individual fraction ages must agree within 2σ error with the "integrated" age of the plateau segment.

4. RESULTS

4.1. Rb-Sr Results

Both the cryptomelane whole-ores and the separates, exhibit relatively low Rb concentrations (19–69 ppm) and higher Sr concentrations (44–659 ppm; Table 1). The two "separate" samples (#28-II and #31-II) that displayed $^{40}Ar/^{39}Ar$ plateau ages (see below) have the lowest Sr contents (less than 100 ppm), with Rb concentrations similar to other samples (around 60 ppm). These results contradict the expectation that the formation of cryptomelane would fractionate the Rb/Sr ratio, as this ratio remains lower than one in all samples.

The clayey matrix is also depleted in Sr (48 ppm), and even more in Rb (2 ppm). The lithiophorite contains respectively 41 and 180 ppm of Rb and Sr.

In spite of these low Rb/Sr ratios, all analyzed cryptomelane samples (whole-ores and separates) have radiogenic strontium isotopic compositions ranging from 0.7449 to 0.8137. $^{87}Sr/^{86}Sr$ ratios of the lithiophorite and the clayey matrix are also within this range. The discrepancy between two analyses of distinct aliquots of sample #34 (0.7466 and 0.7475) indicates the degree of isotopic heterogeneity existing within a sample.

The data do not define an isochron in the Rb-Sr isochron diagram (Fig. 7). However, the results for the whole-ore

TABLE 2. (Continued)

Step n°	$^{40}Ar_{atm.}$ (%)	$^{39}Ar_K$ (%)	$^{37}Ar_{Ca}/^{39}Ar_K$ ($x10^{-4}$)	$^{40}Ar^*/^{39}Ar_K$	Age (Ma)
#28 Cryptomelane (Single grain) (J=0.0164325)					
1	59.7	0.56	0.2064	0.83	24.5 ± 6.5
2	47.2	7.08	0.0769	1.18	34.6 ± 0.8
3	30.7	3.93	0.1414	1.45	42.5 ± 1.0
4	23.4	3.48	0.0674	1.55	45.4 ± 1.6
5	16.0	3.54	0.0226	1.66	48.6 ± 1.0
6	8.7	3.64	0.0016	2.17	63.3 ± 0.8
7	5.3	4.63	0.0082	2.56	74.2 ± 1.0
8	3.9	8.44	0.0419	2.78	80.6 ± 1.4
9	3.1	14.99	0.0814	2.49	72.3 ± 0.3
10	2.2	15.07	0.0190	2.46	71.5 ± 0.4
11	1.3	9.46	0.0427	2.65	76.9 ± 0.5
12	1.2	6.93	0.0506	3.10	89.5 ± 0.7
13	1.4	3.96	0.1433	5.19	147.7 ± 1.2
Fuse	1.3	14.29	0.0265	3.48	100.2 ± 0.5
				Total age:	75.4 ± 0.2
#28-II Cryptomelane (Single grain) (J=0.0164325)					
1	98.5	1.23	0.0554	1.15	33.8 ± 11.2
2	92.4	3.99	0.0253	1.50	43.9 ± 4.6
3	17.2	6.14	0.0109	1.54	45.2 ± 0.7
4	7.2	11.15	0.0080	1.60	46.9 ± 0.4
5	3.5	17.29	0.0080	1.63	47.8 ± 0.4
6	2.7	24.27	0.0080	1.64	47.9 ± 0.3
7	2.9	23.87	0.0074	1.65	48.3 ± 0.3
8	24.8	6.12	0.0071	1.66	48.5 ± 0.8
9	79.7	2.28	0.0223	1.68	49.0 ± 3.6
Fuse	75.4	3.67	0.0126	1.69	49.6 ± 1.9
				Total age:	47.5 ± 0.3
#31 Cryptomelane (Single grain) (J=0.0164325)					
1	49.8	0.00	0.0000	26.24	646.9 ± 2361.5
2	100.0	0.10	-	-	- ± -
3	94.7	1.04	0.0547	1.27	37.3 ± 16.2
4	85.9	1.14	0.0877	1.88	54.8 ± 8.5
5	79.6	1.10	0.0636	2.09	60.8 ± 8.8
6	75.7	1.82	0.0479	2.28	66.4 ± 5.5
7	69.7	2.03	0.0327	2.28	66.3 ± 5.8
8	60.7	2.58	0.0376	2.40	69.7 ± 4.7
9	60.9	2.90	0.0517	2.44	70.8 ± 3.3
10	64.8	2.36	0.0564	2.44	70.9 ± 4.8
11	60.0	4.20	0.0398	2.35	68.4 ± 2.6
12	47.4	5.15	0.0599	2.31	67.1 ± 2.3
13	26.2	7.18	0.0459	2.27	66.0 ± 1.0
14	12.4	11.15	0.0287	2.19	63.6 ± 0.8
15	7.8	17.33	0.0326	2.12	61.8 ± 0.5
16	8.0	13.37	0.0283	2.08	60.6 ± 0.8
17	7.4	13.08	0.0279	2.04	59.4 ± 0.6
18	21.0	4.92	0.0395	1.96	57.1 ± 1.8
Fuse	68.1	8.55	0.0400	1.79	52.2 ± 2.1
				Total age:	61.8 ± 0.5
#31-II Cryptomelane (Single grain) (J=0.0164325)					
1	22.6	0.00	2.8456	5.10	145.1 ± 489.9
2	85.1	0.62	0.0313	0.90	26.4 ± 6.6
3	91.1	1.88	0.0231	1.04	30.7 ± 3.5
4	82.6	1.34	0.0317	1.11	32.6 ± 4.3
5	64.4	1.41	0.0191	1.29	37.8 ± 4.1
6	48.1	1.40	0.0259	1.36	39.8 ± 2.9
7	23.8	2.75	0.0139	1.51	44.3 ± 1.1
8	16.7	6.44	0.0103	1.60	46.7 ± 0.5
9	22.6	9.59	0.0111	1.58	46.2 ± 0.3
10	20.1	12.75	0.0108	1.59	46.6 ± 0.4
11	15.6	9.59	0.0093	1.62	47.3 ± 0.3
12	14.7	10.11	0.0087	1.61	47.1 ± 0.4
13	14.9	11.28	0.0107	1.61	47.1 ± 0.4
14	17.2	10.95	0.0114	1.60	46.7 ± 0.3
15	19.1	8.05	0.0143	1.57	45.9 ± 0.5
16	16.7	3.17	0.0194	1.58	46.1 ± 0.8
Fuse	42.4	8.69	0.0139	1.58	46.2 ± 0.5
				Total age:	45.8 ± 0.2
#32 Cryptomelane (Single grain) (J=0.0164325)					
1	90.1	0.51	0.0932	0.75	22.1 ± 11.9
2	76.1	4.87	0.0105	0.90	26.4 ± 2.0
3	76.8	4.19	0.0185	1.05	30.8 ± 1.6
4	65.2	5.59	0.0179	1.40	41.0 ± 1.7
5	32.0	5.66	0.0259	1.63	47.6 ± 1.4
6	15.2	6.61	0.0283	2.23	65.0 ± 0.9
7	8.2	10.94	0.0080	2.41	70.1 ± 0.8
8	7.1	14.94	0.0084	2.18	63.5 ± 0.5
9	7.1	11.45	0.0097	2.24	65.3 ± 0.5
10	7.7	7.51	0.0090	2.47	71.9 ± 0.7
11	17.3	5.07	0.0196	2.83	82.0 ± 1.2
12	53.3	5.02	0.0175	3.41	98.5 ± 2.2
Fuse	66.2	17.64	0.0111	2.01	58.5 ± 0.9
				Total age:	61.4 ± 0.3
#32-II Cryptomelane (Single grain) (J=0.0164325)					
1	91.2	0.35	0.0141	0.79	23.3 ± 10.7
2	89.1	2.10	0.0257	0.68	20.1 ± 3.9

samples show a positive correlation, corresponding to an age of 2.1 Ga. Three of the separate samples of cryptomelane plot also within this correlation, and are close to their respective whole-ore (Fig. 7). The clayey matrix is also within the same trend. On the other hand, the two samples #28-II and #31-II, with well-defined $^{40}Ar/^{39}Ar$ plateau ages, plot far away to the right of the correlation line, due to their lower Sr contents, and thus, higher, Rb/Sr ratios. Finally, the absence of any mixing line in the $^{87}Sr/^{86}Sr$ vs. 1/Sr diagram (not shown) clearly rules out a simple mixing process.

4.2. $^{40}Ar/^{39}Ar$ Results (Table 2)

Eight whole-ore samples and five separates (veins or concretions labelled by "II"), collected in the different units, were analyzed with the $^{40}Ar/^{39}Ar$ method. The results are illustrated in Figs. 8–13.

4.2.1. Whole ores

All the whole-ore samples display disturbed age spectra. The integrated ages range from 39.8 ± 0.3 Ma to 79.1 ± 0.8 Ma. In spite of the strong disturbances of the age spectra, similar features are found in various samples. (1) All of these samples but one (#7) display some apparent age segments older than 60–65 Ma in their age spectra. (2) Four samples, including the three samples from the clastic ore (#15, #28, and #32) show anomalously high ages in the low to intermediate temperature steps (Fig. 8). (3) These three samples from the clastic horizon, as well as one sample (#22) from the platey level, also show high ages up to 317.5 ± 4.1 Ma in the high temperature steps (Fig. 9). (4) Samples #1 and #34 display age spectra, with younger ages in the range 35–45 Ma, in the high temperature steps (Fig. 10). Sample #7, which is the only sample with all apparent ages lower than 50 Ma (Fig. 10), also shows low ages in the range 16–26 Ma, in the high temperature steps.

A broad age convergence in the intermediate temperature steps is observed around 60–70 Ma, when all age spectra (except #7) are grouped together (Fig. 11). A poorly constrained age cluster between 20 and 40 Ma also appears in the low temperature steps. Furthermore, sample #22 displays a "pseudo" plateau age (less than 70% of the total $^{39}Ar_K$ released) at 67.8 ± 0.8 Ma (Fig. 12).

TABLE 2. (Continued)

Step n°	$^{40}Ar_{atm.}$ (%)	$^{39}Ar_K$ (%)	$^{37}Ar_{Ca}/^{39}Ar_K$ (x10^{-4})	$^{40}Ar^*/^{39}Ar_K$	Age (Ma)
3	96.0	3.97	0.0435	0.88	26.0 ± 4.5
4	85.2	4.50	0.0115	1.13	33.3 ± 3.2
5	77.1	5.18	0.0235	1.10	32.3 ± 1.8
6	62.7	4.48	0.0151	1.36	39.9 ± 1.1
7	43.0	4.91	0.0200	1.63	47.6 ± 0.9
8	19.7	7.62	0.0194	1.80	52.7 ± 0.6
9	11.5	14.91	0.0180	1.90	55.5 ± 0.3
10	10.9	16.60	0.0196	1.96	57.1 ± 0.3
11	11.3	9.16	0.0208	1.95	57.0 ± 0.4
12	13.5	4.41	0.0261	1.85	54.1 ± 0.9
13	13.7	11.29	0.0125	1.86	54.2 ± 0.4
Fuse	25.7	10.53	0.0130	1.86	54.2 ± 0.4
				Total age:	50.0 ± 0.3
#34 Cryptomelane (Single grain) (J=0.0164325)					
1	99.6	0.01	1.7898	0.27	7.9 ± 770.4
2	91.2	1.25	0.0273	1.23	36.0 ± 7.3
3	82.7	2.07	0.0449	1.30	38.1 ± 5.3
4	72.5	2.50	0.0358	1.39	40.6 ± 3.4
5	67.9	5.15	0.0462	1.07	31.5 ± 1.6
6	65.7	5.65	0.0582	0.94	27.5 ± 1.8
7	55.3	6.42	0.0589	1.36	39.8 ± 2.5
8	35.7	7.77	0.0240	2.24	65.3 ± 1.6
9	20.4	10.23	0.0293	2.60	75.4 ± 1.1
10	11.9	12.13	0.0265	2.46	71.5 ± 0.8
11	16.8	10.19	0.0174	2.36	68.5 ± 1.0
12	23.0	9.36	0.0197	2.16	63.0 ± 1.2
13	50.0	8.08	0.0356	1.77	51.7 ± 1.5
Fuse	74.4	19.18	0.0379	1.54	45.2 ± 1.3
				Total age:	55.2 ± 0.5

4.2.2. *Separates*

The age spectra obtained on separates are generally less disturbed than those obtained for the whole-ore samples. Four of the five samples display age spectra with flat segments (Fig. 12). Two real plateau ages at 46.7 ± 0.2 Ma and 48.1 ± 0.2 Ma are obtained for samples #31-II and #28-II, respectively. Two "pseudo" plateau ages (less than 70% of the total $^{39}Ar_K$ released) are displayed by samples #7-II and #32-II, respectively, at 47.3 ± 0.5 Ma and 55.6 ± 0.2 Ma. All of these age spectra present a staircase shape in the low temperature steps, with initial ages in the range 20–40 Ma.

Sample #22-II has the most disturbed age spectrum, with a general staircase shape very similar to that displayed by the corresponding whole-ore (Fig. 12). This age spectrum presents (1) a poorly defined level (one step) at 65.1 ± 0.3 Ma and (2) anomalously high ages in the high temperature steps up to 522.6 ± 4.5 Ma.

4.2.3. *Isochron analysis*

All of the samples were also analysed using $^{36}Ar/^{40}Ar$ vs. $^{39}Ar/^{40}Ar$ correlation diagrams (Turner, 1971; Roddick et al., 1980; Hanes et al., 1985). This analysis confirms the age of the plateaus observed on the age spectra of the separates (Table 3). It also confirms the existence of two poorly constrained "plateau" segments around 36–37 Ma in the low temperature steps, for two whole-ore samples (#7 and #22) (Table 3). The low values of the MSWD (less than 1), are related to the large error bars of the corresponding steps, with high amounts of atmospheric contamination. The high value of the MSWD parameter and the low value of the $(^{40}Ar/^{36}Ar)_i$ ratio of sample #32-II reflect the poor quality of the corresponding plateau segment.

4.2.4. *$^{37}Ar_{Ca}/^{39}Ar_K$ spectra*

Figure 13 shows that no clear relationship can be found between the shape of the $^{37}Ar_{Ca}/^{39}Ar_K$ spectra and the sample type (whole-ore or separate), as previously observed for the age spectra. Nevertheless, the two samples which display the plateau ages around 47 Ma (#28-II and #31-II) also have less disturbed $^{37}Ar_{Ca}/^{39}Ar_K$ spectra, with the lowest (around 0.01) $^{37}Ar_{Ca}/^{39}Ar_K$ ratio values (bold lines in Fig. 13).

5. DISCUSSION

5.1. Rb-Sr data

Our Rb-Sr data clearly indicate that the crystallization of cryptomelane produces a much lower fractionation between Rb and Sr than between K and Ca. Potassium contents range approximately from 1 to 3% in cryptomelanes, while Ca contents are much lower, averaging 0.1–0.2% (Beauvais, 1984). Therefore, K/Rb and Ca/Sr ratios av-

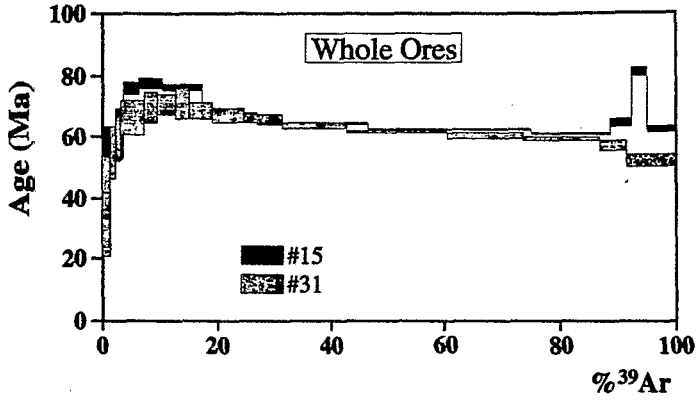

FIG. 8. Two of the four $^{40}Ar/^{39}Ar$ age spectra which display anomalously high ages in the low to intermediate temperature steps. The error bars for each temperature steps are at the 1σ level. The errors in the J-values are not included.

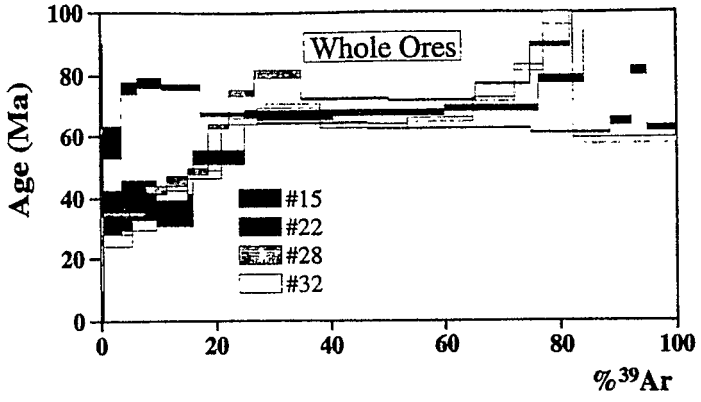

FIG. 9. $^{40}Ar/^{39}Ar$ age spectra with anomalously high ages in the high temperature steps. Same observations as for Fig. 8.

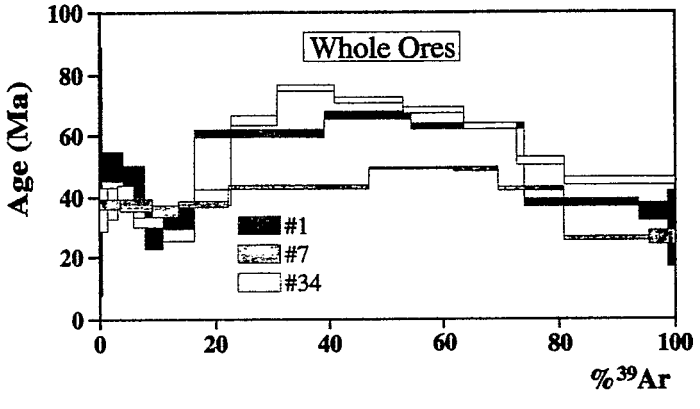

FIG. 10. $^{40}Ar/^{39}Ar$ age spectra with low ages in the low and high temperature steps. Same observations as for Fig. 8.

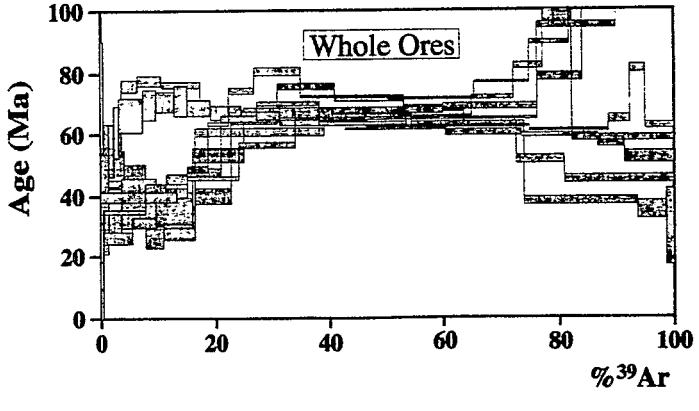

FIG. 11. $^{40}Ar/^{39}Ar$ age spectra of all the whole-ore samples (except sample #7). Same observations as for Fig. 8.

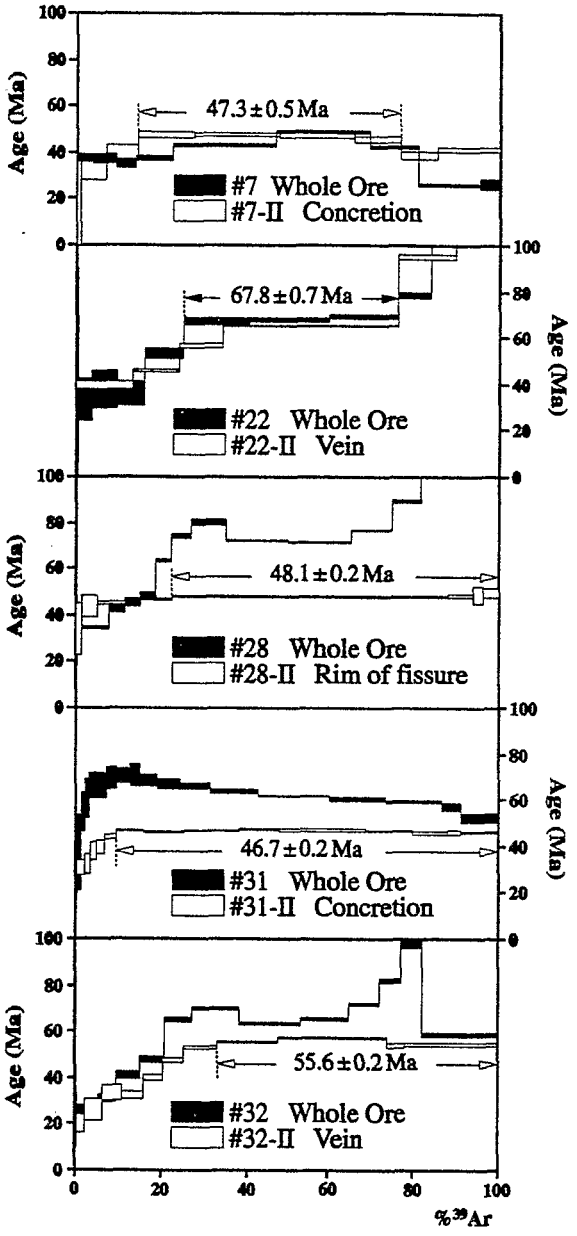

FIG. 12. $^{40}Ar/^{39}Ar$ age spectra of whole-ore and "separate" sample pairs. Same observations as for Fig. 8.

erage ≈500 and ≈10, compared, respectively, to mean crustal values of 200 and 40 (Taylor and McLennan, 1985). These low Ca/Sr ratios probably result from differing behaviour of the two alkaline-earth elements in the cryptomelane structure.

Similarly, Rb/Sr ratios exhibit a wide range of variation between 0.1 and 10 in continental sediments. Cryptomelanes from Azul fall within this range of variation, and consequently, do not show any evidence for a Rb enrichment relative to Sr.

The correlation line obtained in the isochron diagram can be interpreted as a 2.1 Ga reference isochron, in spite of the fact that the Rb-Sr chronometer clearly suffered some perturbation. This age, which corresponds to the formation of the Rio Fresco group containing the Mn protore (Beauvais et al., 1987; Machado et al., 1991; Macambira, 1992) suggests that the Rb-Sr chronometer has not been strongly affected by the first stage of weathering of the proterozoic sediments.

This could result from the presence of inherited phyllosilicates, such as muscovite, occasionally observed in thin sections (Fig. 5) and suggested by some of the $^{40}Ar/^{39}Ar$ results (see below). Nevertheless, traces of muscovite, when present in Mn oxides, cannot fully explain the radiogenic $^{87}Sr/^{86}Sr$.

Consequently, these data suggest that (1) the inherited Sr component is located within the crystal structure of cryptomelanes and (2) the pseudomorphic replacement of rhodochrosite by cryptomelane does not significantly disturb the Rb-Sr chronometer. Neither Rb nor Sr were significantly leached during the first stage of weathering, and both elements probably entered the cryptomelane crystal structure by K-replacement. Thus, this transformation took place in a closed system, at least at the scale of the entire sequence.

This conclusion is supported by the fact that Sr can be integrated within the hollandite crystal structure, (of which cryptomelane is the potassic endmember) (Burns and Burns, 1979), whereas Ca-hollandite has never been described so far. This could explain that Ca, but not Sr, was leached out of the Mn oxides.

Secondary concretions and veins of cryptomelane-2 (#7-II, #32-II, and #22-II) have similar Rb/Sr characteristics to those of whole-ores. This suggests that Sr was not removed during their crystallization. In contrast, the two samples with well-defined $^{40}Ar/^{39}Ar$ plateau ages (#28-II and #31-II) plot far away from the reference isochron (Fig. 7). This clearly indicates that the Rb-Sr system was disturbed during the crystallization of these Mn oxides, with a relative enrichment in Rb.

TABLE 3. Results of the analyses with the $^{36}Ar/^{40}Ar$ vs. $^{39}Ar/^{40}Ar$ correlation diagram method.

Sample	"Plateau" age	Isochron age	$(^{40}Ar/^{36}Ar)_i$	MSWD
#7-II	47.3 ± 0.5	47.1 ± 0.9	299.0 ± 15.9	1.12
#28-II	48.1 ± 0.2	47.8 ± 0.1	298.4 ± 3.0	3.55
#31-II	46.7 ± 0.2	47.1 ± 0.3	285.6 ± 5.5	1.29
#32-II	55.6 ± 0.2	57.0 ± 0.3	256.2 ± 10.1	16.4
#7	37.1 ± 0.8	37.3 ± 1.3	292.6 ± 19.0	0.63
#22	35.8 ± 4.3	37.4 ± 11.0	295.0 ± 3.1	0.04

The $(^{40}Ar/^{36}Ar)_i$ and ages are both calculated from the intercept of the best-fit line (York, 1969), with the respective axis of the correlation plot. MSWD = SUMS/(n − 2); SUMS: weighted sum of residuals; n: number of points fitted.

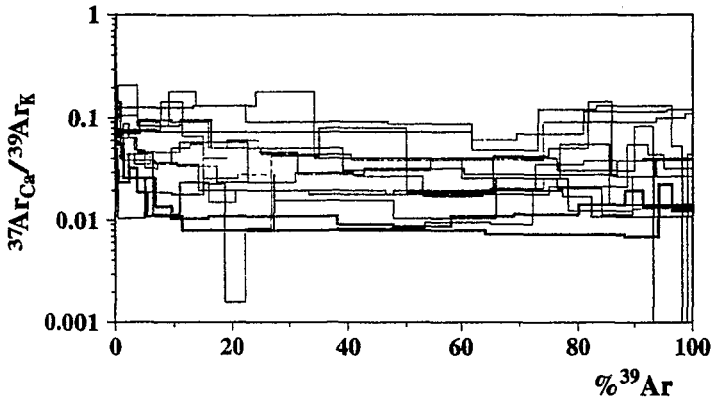

FIG. 13. $^{37}Ar_{Ca}/^{39}Ar_K$ spectra of all the studied samples. Black lines: $^{37}Ar_{Ca}/^{39}Ar_K$ spectra of samples #28-II and #31-II; Grey lines: all others $^{37}Ar_{Ca}/^{39}Ar_K$ spectra.

Unlike in the first generation, the initial textures were not preserved during the crystallization of these samples (Fig. 3), leading to much lower Sr contents in these minerals.

The two-point isochrons drawn between whole-ore samples and separates correspond to unrealistic ages of 351 and 93 Ma, much older than the $^{40}Ar/^{39}Ar$ ages. These results indicate that sample pairs formed by whole-ores and veins or concretions were not closed-systems for Rb and Sr after formation. This may result either from initial isotopic inhomogeneities between whole-ores and veins or concretions, or from continuous chemical exchange after formation.

5.2. $^{40}Ar/^{39}Ar$ Data

5.2.1. Age spectra shapes

One of the significant features of the age spectra, mainly for whole-ore samples, is that anomalously low or high ages are often observed within a spectrum, in the low or high temperature steps, respectively.

The low ages in the low temperature steps are observed for almost all the age spectra, often with a staircase shape in the first 10–20% of the total $^{39}Ar_K$ released.

Low ages in the high temperature steps are also observed in three age spectra: #1, #7, and #34 (Fig. 10). Furthermore, samples #7-II and #31 (Figs. 12, 8) also show, to a lesser extent, slightly younger ages in the final stages of degassing of $^{39}Ar_K$. When the low ages occur both in the low and high temperature steps, the resulting age spectrum has an upward-convex shape (#1, #7, #34) (Fig. 10).

These low ages are generally correlated to higher $^{37}Ar_{Ca}/^{39}Ar_K$ ratios. Low ages in the low temperature steps, combined with high $^{37}Ar_{Ca}/^{39}Ar_K$ ratios are frequently observed for other kinds of minerals and are generally explained by the presence of poorly crystallized alteration phases. However, this hypothesis cannot explain the low ages in the high temperature steps, as these alteration phases release their radiogenic Ar in a lower temperature domain than that of the "primary" minerals. On the other hand, convex-upward age spectra have been found in white micas (e.g., Wijbrans and McDougall, 1986) and were interpreted as indicating the presence of two mixed white mica generations with distinct isotopic closure ages. These authors explained the lowering of the apparent ages in the initial and final degassing steps by a larger temperature span of the degassing spectrum of the youngest mica generation. This hypothesis can also be invoked to explain the convex-upward age spectra displayed by some of our cryptomelane samples.

The distinct ages which are found in the low and high temperature steps (e.g., #34) (Fig. 10) can be explained either by distinct overlaps of the degassing spectra in the two temperature domains or by the presence of an alteration phase which preferencially degasses in the low temperature steps. Whatever the case, the highest ages of the age-spectra bumps give a minimum estimate of the true age of the oldest manganese oxide generation (see for instance samples #7 and #7-II, which display concordant ages in the intermediate temperature steps and discordant ages outside this temperature domain (Fig. 12)).

Four samples display age spectra with higher ages in the low (#15 and #31) (Fig. 8) or intermediate temperature steps (#28 and #32) (Fig. 9). The latter samples also show steep staircase shapes for the first 25% of the total $^{39}Ar_K$ released. A common problem of the $^{40}Ar/^{39}Ar$ dating method is the loss by recoil of neutron irradiation-generated $^{39}Ar_K$, especially when the material studied is very fine-grained (Turner and Cadogan, 1974; Harrison, 1983; Foland et al., 1992). Classically, the age spectrum displays old apparent ages, due to the $^{39}Ar_K$ loss, in the low temperature steps, followed by a slow decreasing staircase shape of the apparent ages towards higher temperature steps (Turner and Cadogan, 1974). Samples #15 and #31 (Fig. 8) display age spectra which correspond exactly to this model, except for the lowest temperature steps. In these two samples, the $^{39}Ar_K$ displaced during the n,p transmutation definitely left the irradiated system, since low ages are observed only in the very first steps, corresponding only to a few percents of the total $^{39}Ar_K$ released. By contrast, low ages in the low temperature steps are observed in a larger degassing domain of samples #28 and #32 (Fig. 9). This may result from the incorporation of the displaced $^{39}Ar_K$ from the K-rich Mn oxides into other K-poor Mn oxides or alteration phases. In these samples, disturbed by $^{39}Ar_K$ recoil, the decreasing staircase shape of the age spectra in the intermediate to high temperature steps displays apparent ages

which tend towards, and may eventually reach, the true age of the mineral. Vasconcelos et al. (1994) did not observed any direct evidence of recoil in their samples. This may result from the large atmospheric contamination in the low to intermediate temperature steps of their experiments, which may hide the recoil effects, and which did not occur in our samples for some unknown reason.

Five of our samples (#15, #22, #22-II, #28, #32) (Figs. 9, 12) give unrealistically old ages in the high temperature steps, which may reflect the presence of inherited hypogene minerals, such as muscovite or K-feldspar, as also revealed by the petrographic observation (Fig. 5). Indeed, muscovite releases its radiogenic argon in an higher temperature domain than cryptomelane (or other Mn oxides) (Vasconcelos et al., 1994).

5.2.2. *Chronological implications*

In addition to the methodological questions discussed above, five observations remain to be discussed which are relevant to the chronology of evolution of the Azul Mn ore:

1) All whole-ore age spectra (except that of sample #7) show an age convergence around 60–70 Ma in the intermediate temperature steps (Fig. 11).
2) The age spectra displayed by the "separate" samples are less disturbed and give different ages than those of the corresponding whole-ores (Fig. 12).
3) One of the "separate" sample (#32-II) displays a poorly constrained plateau age at 55.6 ± 0.2 Ma (Fig. 12).
4) Very good plateau ages are displayed by three separate samples (#28-II, #7-II, #31-II). These ages are concordant within error bars and allow calculation of a mean value of 47.4 ± 0.1 Ma (Fig. 12).
5) Three whole-ore samples display low ages around 37 Ma in the low (#7, #22) or in the high (#1) temperature steps (Figs. 9, 10).

Vasconcelos et al. (1994) defined three age clusters for the Azul Mn-ore, respectively, at 65.5–68 Ma, 51–56 Ma, and 40–43 Ma. They proposed that these age clusters characterize the episodic precipitation of the three successive Mn-oxide generations of the Azul Mn deposit as a result of superimposed weathering events.

Our data confirm that cryptomelane-1 probably formed between 60 and 70 Ma as proposed by Vasconcelos et al. (1994). We find evidence for some Early Paleocene-Upper Cretaceous ages in all the whole-ore samples (except #7) (Figs. 11, 14) and one separate sample (#22-II). Furthermore, one whole-ore age spectrum (#22) displays a plateau segment at 67.8 ± 0.8 Ma (51% of the total $^{39}Ar_K$ released) (Fig. 12). This age cluster is not very well constrained, probably because whole-ore samples are mixtures of cryptomelane and other constituents, unlike separates which are primarily composed of cryptomelane. The lower ages in the low or high temperature steps may be related to the presence of younger cryptomelane generations in the whole-ore samples, as discussed above.

The age at 55.6 ± 0.2 obtained for the separate sample #32-II is only constrained by one sample, and the plateau age is of poor quality. Nevertheless, this result is concordant with the age cluster at 51–56 Ma defined by Vasconcelos et al. (1994) for the Azul area (Figs. 12, 14).

The most reliable ages, according to the usual criteria of the $^{40}Ar/^{39}Ar$ method (see above), are displayed by the three "separate" samples. These early Eocene ages, with a mean value at 47.4 ± 0.1 Ma are clearly distinct from the two age clusters (51–56 Ma and 40–43 Ma) that were attributed respectively to the second and third cryptomelane genera-

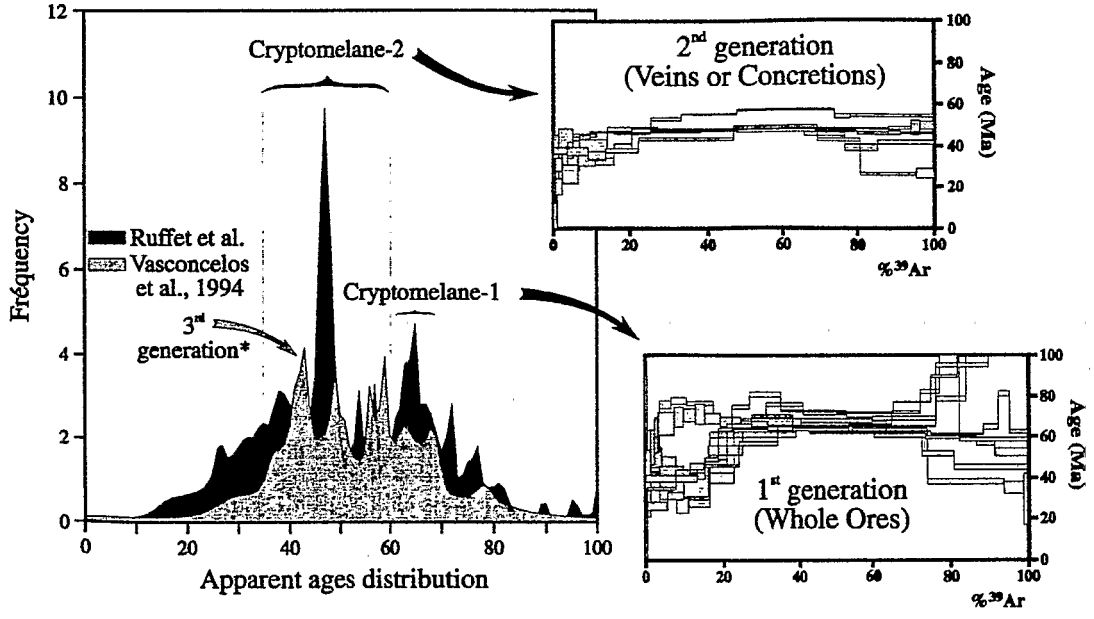

FIG. 14. Distribution of all the apparent ages (step-heating increments) of the age spectra from this study (black) and from the study (Azul area) of Vasconcelos et al. (1994) (light grey). The age spectra of the second cryptomelane generation do not include sample #22-II, whereas the age spectra of the first cryptomelane generation do not include sample #7. *: third cryptomelane generation (or cryptomelane-3) defined by Vasconcelos et al. (1994).

tions by Vasconcelos et al. (1994) (Figs. 12, 14). Moreover, these separate samples are essentially composed of the second generation of cryptomelane. As emphasized above, no occurence of the third cryptomelane generation described by Beauvais et al. (1987) or Vasconcelos et al. (1994) has been detected in the samples of this study. We nevertheless obtained low ages (around 37 Ma) from three whole-ore samples (Figs. 9, 11, 14).

Therefore, we believe that these results contradict the model proposed by Vasconcelos et al. (1994), which proposes that each cryptomelane generation corresponds to distinct weathering events corresponding to global climatic changes. Cryptomelane-2 and -3 may have formed simultaneously and more or less continuously over several million years (from 56 Ma to 40 and possibly 37 Ma). This interpretation seems more compatible with the petrographic evidence that each generation of Mn oxide replaces progressively the previous generation through dissolution and in situ recrystallization. Although the mineralogical "evolutionary sequence" suggests a gradation from bottom to top of the profiles and from upstream to downstream of the sequence, this does not imply a simple spacial nor temporal spacing of crystallization events. Because of the complex path of water circulation and residence time within the profiles, the crystallization of the different generations of cryptomelane may occur sequentially at a given location, but simultaneously at different locations in the profile. In fact, no simple correlation is observed between sample depth and the age or shape of the $^{40}Ar/^{39}Ar$ age spectra (see for instance, samples #1, #7, and #15 (Figs. 8, 10), collected at different depth in profile A1P 170).

A final noticeable feature of the Azul chronology is that the formation of cryptomelane seems to have stopped much earlier than at other locations in Brazil. The youngest age found by Vasconcelos et al. (1994) is 41 ± 2 Ma. More recent crystallization events may have occurred, as indicated by the few age segments at 37 Ma displayed by some of our whole-ore samples. Nevertheless, these lower Eocene ages are much older than those found in the Igarapé Bahia profile (Carajàs mountains) (Vasconcelos et al., 1994). This difference remains to be explained, and is most likely associated with local factors rather than continental-scale climate changes. One hypothesis involves a decrease of K available for recrystallization in the Mn-protore, due to exhaustion of the original K-bearing minerals in the parent rock. Systematic budget calculations, as well as comparisons with other locations in the same continental area will have to be carried out to solve this problem.

6. CONCLUSIONS

1) These results show that cryptomelane is a suitable mineral for dating with the $^{40}Ar/^{39}Ar$ method as previously proposed by Vasconcelos et al. (1994). However, problems related to ^{39}Ar recoil during neutron irradiation, contamination by hypogene phases, or the presence of multiple generations of Mn-oxides are encountered.

2) Fine-scale sampling allowed by the laser probe $^{40}Ar/^{39}Ar$ technique makes it possible to analyse separately distinct generations of Mn oxides extracted from a single sample. The most reliable ages were obtained on separates, either millimetric veins crosscutting the samples or millimeter-thick concretions covering the faces of fissures.

3) Little Rb/Sr fractionation occurs during cryptomelane crystallization. Large variations of the $^{87}Sr/^{86}Sr$ ratio are found among the samples, inherited from the 2.1 Ga old parent rock. This shows that little isotopic homogenization occurred during the crystallization of the Mn oxides, which, thus, cannot be dated by the Rb/Sr method.

4) Our data confirm that the oldest and first cryptomelane generation (cryptomelane-1), formed by pseudomorphic replacement of rhodocrosite, probably developed between 60 and 70 Ma.

5) Some of the samples of the second cryptomelane generation displayed ages around 47 Ma, distinct from the two age clusters at 51–56 and 40–43 Ma defined by Vasconcelos et al. (1994). Furthermore, hints of younger ages, around 37 Ma, without any evidence of a third cryptomelane generation, are observed in the age spectra of some of our samples.

6) These results suggest, in contradiction with the interpretation of Vasconcelos et al. (1994), that the evolution of Mn oxides and cryptomelane in the weathering profile essentially results from a continuous process and that successive petrographic generations may form simultaneously within one profile.

7) Although the previous conclusion may put some limitations to the use of the K-Mn oxides as paleoclimatic "tracers", the $^{40}Ar/^{39}Ar$ study of these minerals provides, nevertheless, the first absolute radiochronological constraints on the development of tropical weathering. This invaluable information will clearly be extremely useful in the near future, for paleoalteration studies and for more precisely understanding both the mechanisms and timing of laterite formation.

Acknowledgments—This work has been founded by the INSU–ORSTOM program PEGI (Programme d'étude de la géosphère intertropicale). J. J. Motte and R. Dassule are thanked for drawing some of the figures. W. Barthelemy is acknowledged for technical assistance in the solid source mass spectrometry. E. Brown is greatly thanked for correcting the manuscript.

Editorial handling: K. R. Ludwig

REFERENCES

Alibert C., Michard A., and Albarède F. (1983) The transition from alkali basalts to kimberlite: isotope and trace element evidence from melilitites. *Contrib. Mineral. Petrol.* **82,** 176–186.

Beauvais A. (1984) Concentrations manganésifères latéritiques. Etude pétrologique de deux gîtes sur roches sédimentaires précambriennes. Gisements de Moanda (Gabon) et d'Azul (Brésil). Thèse d'Université (Poitiers).

Beauvais A., Melfi A., Nahon D., and Trescases J. J. (1987) Pétrologie du gisement latéritique manganésifère d'Azul (Brésil). *Mineral. Deposita* **22,** 124–134.

Bernardelli A. and Beisiegel V. R. (1978) Geologia economica da jazida de manganes do Azul. *An. XXX Congr. Bras. Geol.* **4,** 1431–1444.

Bricken O. (1965) Some stability relations in the system $Mn–O_2–H_2O$ at 25 and one atmosphere total pressure. *Amer. Mineral.* **50,** 1296–1354.

Burns R. G. and Burns V. M. (1979) Manganese oxides. In *Marine Minerals* (ed. P. H. Ribbe); *Rev. Mineral.* 1–46.

Clauer N., Giblin P., and Lucas J. (1984) Strontium and Ar isotope studies of detrital smectites from the Atlantic Ocean (D.S.D.P., legs 43, 48 and 50). *Chem. Geol.* **2,** 141–151.

Clauer N., Chaudhuri S., Kralik M., and Bonnot-Courtois C. (1993) Effects of experimental leaching on Rb-Sr and K-Ar isotopics systems and REE contents of diagenitic illite. *Chem. Geol.* **103,** 1–16.

Foland K. A., Hubacher F. A., and Arehart G. B. (1992) $^{40}Ar/^{39}Ar$ dating of very fined grained samples: An encapsuled-vial procedure to overcome the problem of ^{39}Ar recoil loss. *Chem. Geol.* **102,** 269–276.

Garrels R. M. and Christ C. L. (1965) *Solutions, Minerals and Equilibria.* Freeman Cooper & Company.

Giovanoli R. and Leuenberger V. (1969) Uber die oxidation von manganoxihydroxide. *Helvetica Chim. Acta* **52,** 2333–2347.

Hanes J. A., York D., and Hall C. M. (1985) An $^{40}Ar/^{39}Ar$ geochronological and electron microprobe investigation of an Archean pyroxenite and its bearing on ancient atmospheric compositions. *Can. J. Earth. Sci.* **22,** 947–958.

Harrison T. M. (1983) Some observations on the interpretation of $^{40}Ar/^{39}Ar$ age spectra. Isotope *Geoscience* **1,** 319–338.

Herz N. and Banerjee S. (1973) Amphibolites of the lafaiete, Minas Gerais, and the Serra Do Navio Manganese Deposits, Brazil. *Econ. Geol.* **68,** 1289–1296.

Hypólito R., Valarelli J. V., Giovanoli R., and Netto S. M. (1984) Gibbs free energy of formation of synthetic cryptomelane. *Chimia* **38,** 427–429.

Macambira M. (1992) Chronologies U–Pb, Rb/Sr, K/Ar et croissance de la croûte continentale dans l'Amazonie du Sud-Est; exemple de la région de Rio Maria, province de Carajàs, Brésil. Thesis, Univ. Montpellier II.

Machado N., Lindenmayer Z., Krogh T. E., and Lindenmayer D. (1991) U–Pb geochronology of archen magmatism and basement reactivation in the Carajas area, Amazon shield, Brazil. *Precambrian Res.* **49,** 329–354.

Merino E., Nahon D., and Wang Y. (1993) Kinetics and mass transfer of pseudomorphic replacement: application to replacement of parent minerals and kaolinite by Al, Fe and Mn oxides during weathering. *Amer. J. Sci.* **293,** 135–155.

Morton J. P. and Long L. E. (1980) Rb-Sr dating of paleozoic glauconite from the Llano region, Central Texas. *Geochim. Cosmochim. Acta* **44,** 663–672.

Nahon D. and Parc S. (1990). Lateritic concentrations of manganese oxyhydroxides and oxides. *Geolg. Rundsch.* **79,** 2, 319–326.

Nahon D., Beauvais A., Nziengui-Mapangou P., and Ducloux J. (1984) Chemical weathering of Mn-garnets under lateritic conditions in Northwest Ivory coast (West Africa). *Chem. Geol.* **45,** 53–71.

Nziengui-Mapangou P. (1981) Pétrologie comparée de gisements manganésifères supergènes en Afrique (gisement de Ziémougoula en Côte d'Ivoire et gisement de Moanda au Gabon). Thesis Univ. of Poitiers unpubl.

Parc S., Nahon D., Tardy Y., and Vieillard P. (1989) Estimated solubility and fields of stability for cryptomelane, nsutite, birnessite and lithiophorite based on natural lateritic weathering sequences. *Amer. Mineral.* **74,** 466–475.

Perseil E. A. and Grandin G. (1985) Altération supergène des protores à grenats manganésifères dans quelques gisements d'Afrique de l'Ouest. *Mineral. Deposita* **20,** 211–219.

Post J. E., Von Dreele R. B., and Buseck P. R. (1982) Symmetry and cation displacements in Hollandites: structure refinements of Hollandite, Cryptomelane and Priderite. *Acta Cryst.* **B38,** 1056–1065.

Roddick J. C., Cliff R. A., and Rex D. C. (1980) The evolution of excess argon in alpine biotites-A ^{40}Ar-^{39}Ar analysis. *Earth Planet. Sci. Lett.* **48,** 185–208.

Ruffet G., Féraud G., and Amouric M. (1991) Comparison of ^{40}Ar-^{39}Ar conventional and laser dating of biotites from the North Trégor Batholith. *Geochim. Cosmochim. Acta* **55,** 1675–1688.

Samson S. D. and Alexander E. C., Jr. (1987) Calibration of the interlaboratory ^{40}Ar-^{39}Ar dating standard, MMhb-1. *Chem. Geol.* **66,** 27–34.

Scaillet S., Féraud G., Lagabrielle Y., Ballèvre M., and Ruffet G. (1990) ^{40}Ar-^{39}Ar laser-probe dating by step-heating and spot fusion of phengites from the Dora Maira nappe of the Western Alps, Italy. *Geology* **18,** 741–744.

Staudigel H., Gillis K., and Duncan R. (1986) K-Ar and Rb-Sr ages of celadonites from the Troodos ophiolite. *Geology* **14,** 72–75.

Steiger R. H. and Jäger E. (1977) Subcommission on geochronology: convention on the use of decay constants in geo- and cosmochronology. *Earth Planet. Sci. Lett.* **36,** 359–362.

Taylor S. R. and McLennan S. M. (1985) *The Continental Crust/its Composition and Evolution; Geoscience texts.* Blackwell.

Turner G. (1971) ^{40}-^{39}Ar ages from the lunar Maria. *Earth Planet. Sci. Lett.* **11,** 169–191.

Turner G. and Cadogan P. H. (1974) Possible effects of ^{39}Ar recoil in ^{40}Ar-^{39}Ar dating. *Proc. 5th Lunar Conf.* **2,** 1601–1615.

Vasconcelos P. M., Renne P. R., Brimhall G. H., and Becker T. A. (1994) Direct dating of weathering phenomena by ^{39}Ar-^{40}Ar and K-Ar analysis of supergene K-Mn oxides. *Geochim. Cosmochim. Acta* **58,** 1635–1665.

Vicat J., Fanchon E., Strobel P., and Qui D. T. (1986) The structure of $K_{133}Mn_8O_{16}$ and cation ordering in hollandite-type structures. *Acta Cryst.* **B42,** 162–167.

Wijbrans J. R. and McDougall I. (1986) $^{40}Ar/^{39}Ar$ dating of white micas from an Alpine high-pressure metamorphic belt on Naxos (Greece): the resetting of the argon isotope system. *Contrib. Mineral. Petrol.* **93,** 187–194.

York D. (1969) Least squares fitting of a straight line with correlated errors. *Earth Planet. Sci. Lett.* **5,** 320–324.

APPENDIX

1) AIP 170 profile

a) #1, collected in the indurated Mn-ore level, is composed of black cryptomelane with some nsutite and small layers of grey pyrolusite. The whole sample was analyzed, since it was not possible to separate the different phases.

b) #7 was also collected in the indurated Mn-ore level. The massive ore (#7) contains principally cryptomelane and nsutite. Cryptomelane-2 appears as disseminated brown concretions (#7-II), which were separated and analyzed separately.

c) #15 was sampled in the clastic ore. The ore itself (#15) is composed of small exfoliated plates and blocks, made of cryptomelane with very little nsutite, packed in a reddish, clayey matrix (#15-III) made of kaolinite and minor gibbsite.

2) AIP 175 profile

#22 was collected in the little indurated ore. The ore (#22) is bluish to black, and is very rich in cryptomelane. Veins of cryptomelane-2 (#22-II) crosscut the platey layering. Lithiophorite has (#22-III) crystallized in the ore cavities.

3) AIP 163 profile

#28 was collected in the clastic ore. It is composed of consolidated, cemented plates (#28), crosscut by a system of small fractures filled by secondary minerals, in which grey-coloured, cryptomelane-2 has been recognized (#28-II).

4) AIP 162 profile

#31 was collected in the poorly consolidated ore. The ore (#31) is blue to blackish, and plates are cemented. Cryptomelane constitutes the main mineral species, and is associated with nsutite. Brown concretions of cryptomelane-2 (#31-II) may also be observed.

5) Samples collected out of the weathering profiles

#32 was sampled at the surface level in the Mn mine and is issued from the clastic ore. The ore (#32) is very rich in cryptomelane. A crosscutting vein of cryptomelane-2 (#32-II), separated from the ore, was also analyzed.

#34 was sampled in a cross-section along a cutting. The sample is blue to grey and belongs to the poorly consolidated ore. Two phases can be distinguished. Both are enriched in cryptomelane, with also nsutite and kaolinite. We only analyzed the whole-ore.